

A Highly Efficient Metal-Free Oxygen Reduction Electrocatalyst Assembled from Carbon Nanotubes and Graphene

Jia Yang, Haiyan Sun, Haiyi Liang, Hengxing Ji, Li Song, Chao Gao,* and Hangxun Xu*

The oxygen reduction reaction (ORR) at the cathode is an important process for many state-of-the-art energy storage and conversion devices that operate in alkaline (e.g., metal–air batteries, alkaline fuel cells, chlor-alkali electrolyzers, etc.) or acidic (e.g., proton-exchange-membrane fuel cells) media. However, the ORR is a kinetically sluggish reaction which greatly affects the chemical-electrical energy conversion efficiency.^[1–4] So far, Pt-based electrocatalysts are generally considered as the best catalysts for ORR.^[5–8] The high cost and scarcity of Pt-based materials, however, significantly limit the large-scale commercialization of the above technologies. In addition, Pt-based electrocatalysts still suffer from insufficient durability and poor tolerance against carbon monoxide poisoning and methanol crossover.^[9–11] Therefore, much effort has been devoted to developing non-Pt materials as efficient, durable, and low-cost electrocatalysts to substitute Pt-based materials for ORR.^[12–23]

Heteroatom-doped carbons represent one of the most promising electrocatalysts for ORR due to their inherently unique electronic and structural properties.^[24–28] Through careful selection of carbon precursors and optimization of the carbon nanostructures, significant progress has been achieved in developing heteroatom-doped carbon materials as metal-free electrocatalysts for ORR.^[29–41] In principle, crystalline carbons such as carbon nanotubes (CNTs) and graphene with good electrical conductivities, excellent mechanical strengths, and large surface areas are very promising candidates for advanced ORR electrocatalysts.^[24] However, the ORR performance for many of the heteroatom-doped electrocatalysts based on CNTs or graphene is still inferior to the commercial Pt/C catalyst, nonprecious-metal catalysts, or even noncrystalline micro/mesoporous carbon-based materials. This could be attributed to the fact

that CNTs prefer to form bundles and graphene nanosheets can easily restack with each other. Hence, their intrinsically unique physical properties are not fully exploited for preparing high-performance electrocatalysts. Recently, assembling CNTs with graphene to form CNT/graphene hybrid materials has been demonstrated to be an effective way to prevent stacking of CNTs and graphene.^[42,43] Electrochemical measurements show that CNT/graphene hybrid materials have better electrochemical performance than that only consisted of CNTs or graphene.^[42–47] Until now, facile and effective methods to integrate CNTs and graphene, which can yield hybrid materials with new structural characteristics and prominent electrocatalytic activity for ORR, are still rare and remain challenging.^[42,43,47] In addition, the synthetic strategies currently used for synthesizing ORR catalysts are generally difficult or impossible to scale up, which poses another great challenge for realizing the large-scale practical application of fuel cells and other energy conversion devices.^[1,48] Therefore, it is highly desirable to develop a synthetic approach to produce highly efficient electrocatalysts for ORR in a scalable and continuous manner.

Here, we demonstrate a one-step aerosol route to facile assemble CNTs and graphene into hybrid nanospheres (CGHNs). In this aerosol approach, assembly of CNTs and graphene into CGHNs can prevent the formation of CNT bundles and restacking of individual graphene sheets, effectively increasing the specific surface area. The crumpled graphene surfaces can also increase the reactive sites for ORR. Due to strong π - π interaction between CNTs and graphene, the CGHNs are highly stable. Furthermore, such a hybrid structure could form efficient charge transfer pathways with synergistically improved electronic conductivity. All above characteristics are favorable for enhancing the ORR activity. After doping with nitrogen and phosphorus, as-obtained hybrid nanospheres (N,P-CGHNs) with optimized structure exhibit superior ORR performance to the commercial Pt/C catalyst (20 wt% Pt, Johnson Matthey) in alkaline solution. While previous metal-free catalysts are generally less effective toward ORR in acidic solution, our N,P-CGHNs are found to show comparable catalytic activity to Pt/C and exhibit even better performance after 5000 cycles in 0.1 M HClO₄. Control experiments show that N,P-CGHNs prepared using the aerosol method exhibit much higher ORR performance than N,P-doped CNT/graphene hybrid materials synthesized using hydrothermal and sol-cryo methods.^[42,49] Furthermore, the performance of Zn–air batteries fabricated with N,P-CGHNs can outperform the commercial Pt/C catalyst. The highly efficient electrocatalyst assembled from CNTs and graphene via aerosol route is therefore a promising replacement for Pt-based materials in many important electrochemical

J. Yang, Prof. H. Liang, Prof. H. Ji, Prof. L. Song,
Prof. H. Xu
CAS Key Laboratory of Soft Matter Chemistry
Department of Polymer Science and Engineering
Department of Modern Mechanics
Department of Materials Science and Engineering
National Synchrotron Radiation Laboratory
University of Science and Technology of China
Hefei, Anhui 230026, P. R. China
E-mail: hxu@ustc.edu.cn

Dr. H. Sun, Prof. C. Gao
MOE Key Laboratory of Macromolecular Synthesis and Functionalization
Department of Polymer Science and Engineering
Zhejiang University
Hangzhou, Zhejiang 310027, P. R. China
E-mail: chaogao@zju.edu.cn



DOI: 10.1002/adma.201505855

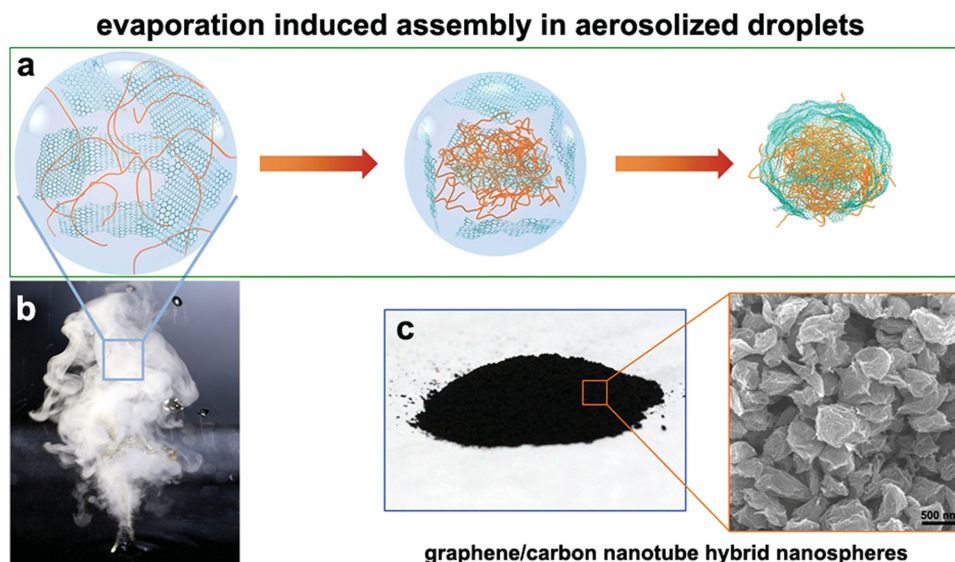


Figure 1. a) Schematic illustration of the process for co-assembling carbon nanotubes and graphene into hybrid nanospheres in rapidly evaporating aerosol droplets. b) A photograph of the ultrasonic fountain and mist generated by a high-frequency ultrasound (1.7 MHz) from an aqueous dispersion containing oxidized carbon nanotubes and graphene oxides. c) A photograph and corresponding SEM image of the black powder collected from the filter after aerosol processing.

energy conversion devices, including metal-air batteries and fuel cells.

Figure 1a shows our procedure to fabricate CGHNs by assembling CNTs and graphene in rapidly evaporating droplets (the experimental setup is schematically shown in Figure S1, Supporting Information). The aqueous solutions containing oxidized CNTs and graphene oxides (GOs) with a total concentration of 2 mg mL^{-1} were nebulized to generate aerosol droplets that flowed through a tube furnace preheated at $350 \text{ }^\circ\text{C}$. Micron-sized droplets generated by high-frequency ultrasound (1.7 MHz) containing well dispersed oxidized CNTs and GOs (Figure 1b) were transformed into black powders consisting of individual nanospheres with crumpled textures (Figure 1c). The apparatus is simple, continuous, and easily scaled up to mass production.^[50] The final structure can be controlled by varying the stoichiometric amounts of oxidized CNTs and GOs in the precursor solution.

The structure and morphology of as-obtained hybrid materials were first examined using scanning electron microscopy (SEM) and high-resolution transmission electron microscopy (HRTEM). As shown in Figure S2a,c (Supporting Information), aerosolization of oxidized CNTs produced entangled nanospheres with folded and twisted CNTs. Meanwhile, aerosolization of GOs can lead to the formation of crumpled graphene nanospheres, consistent with previous reports (Figure S2b,d, Supporting Information).^[51,52] Interestingly, when mixtures of oxidized CNTs and GOs with different mass ratios were nebulized and passed through the furnace, CGHNs with an average size around 500–800 nm were obtained as shown in **Figure 2a–c**. Particularly, the fibrillar structure could not be observed in CGHNs compared to the pure CNT nanospheres (Figure S2a, Supporting Information), indicating graphene sheets formed a thin outer layer which can be clearly revealed from HRTEM images (Figure 2d–f). HRTEM images also show that the thickness of graphene coating directly correlates to the

content of GOs in the mixtures of oxidized CNTs and GOs. For hybrid nanospheres prepared from 1:5 mass ratio of CNTs to GOs, there are five to six graphene outer layers coated on CNTs (Figure 2g). When the mass ratio of CNTs to GOs varies from 1:5 to 1:1, the number of graphene layers decreases to ≈ 3 (Figure 2h). Further decreasing the GO content leads to the formation of only one to two graphene layers coated on CNTs (Figure 2i). By contrast, there are eight to ten layers of graphene in crumpled graphene nanospheres (Figure S2f, Supporting Information).

This unique CNT/graphene hybrid nanostructure obtained from aerosol process is likely caused by the different thermodynamic behaviors of the oxidized CNTs and GOs in rapidly evaporating droplets. GOs are known to preferentially aggregate at the solvent/gas interface due to their amphiphilic and flexible nature in aqueous solutions.^[53] Meanwhile, the large hydrodynamic size of GOs also slows their movement from the drying front. GOs, thus, accumulate as a multilayer film at the droplet outer surface and collapse by capillary force at the late stage of drying as observed in previous cargo-filled graphene nanosacks.^[54–56] By contrast, oxidized CNTs, which have the same negative surface charge as GOs, tend to diffuse away from the drying front and localize in the interior of drying droplets due to their 1D fibrillar structure. Therefore, CNTs and GOs spontaneously segregate into CGHNs. This evaporation-induced assembly approach is simple yet effective, with a very short processing time of several seconds.^[50–52] More importantly, it can be operated in a continuous manner, avoiding batch-to-batch variations.

X-ray photoelectron spectroscopy (XPS) indicated that the oxygen content in CGHNs decreased after aerosol processing (Table S1, Supporting Information). Since CNT and GOs were only partially reduced, some surface functional groups such as carboxyl, carbonyl, and epoxy groups were still present in CGHNs as commonly seen in oxidized carbon materials.

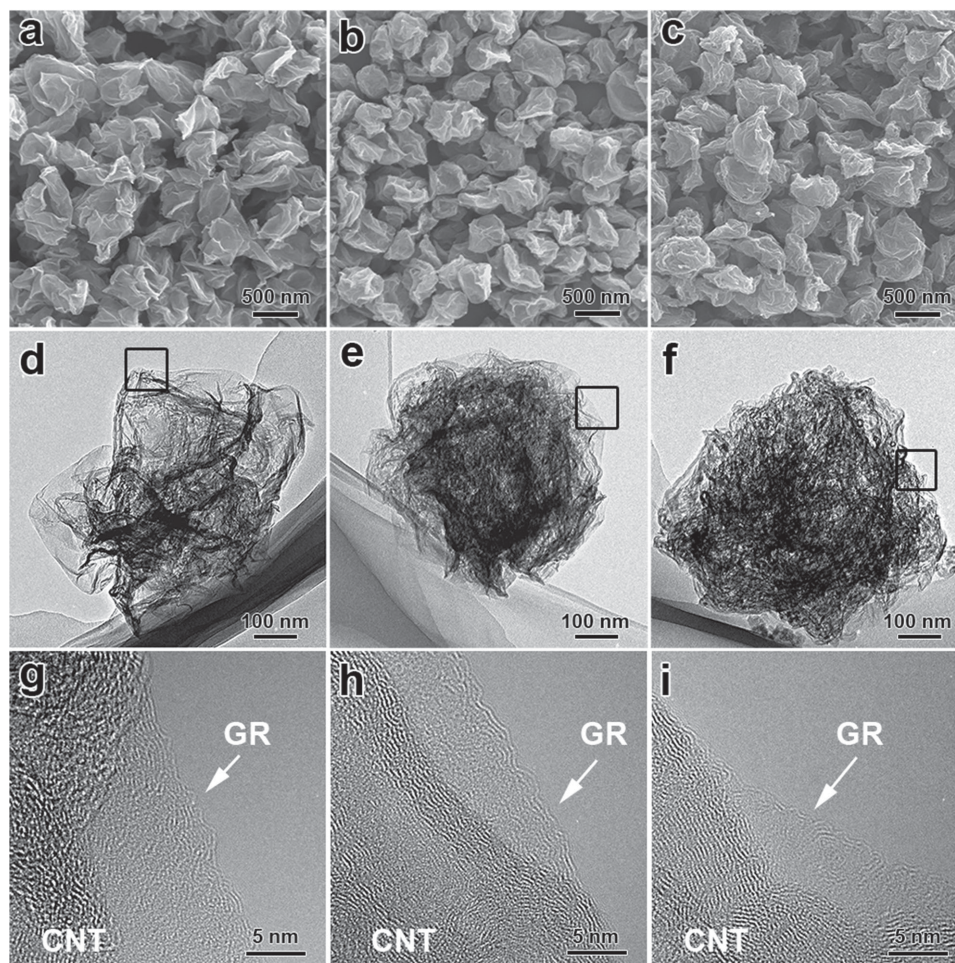


Figure 2. SEM and HRTEM images of CGHNs obtained from different mass ratios of CNT/graphene: (a,d) 1:5, (b,e) 1:1, and (c,f) 5:1. g–i) Enlarged HRTEM images as indicated by the black squares in (d–f).

For example, deconvoluted C 1s peak (Figure S3, Supporting Information) indicated the presence of C–O (286.5 eV), C=O (288 eV), O=C=O (289 eV) groups in CGHNs assembled from 1:1 mass ratio of CNT/graphene. These oxygen-containing groups are crucial for following doping process as they can react with dopants and form new heteroatom-containing active sites. Incorporation of heteroatoms (e.g., B, N, S, P) into a carbon skeleton could effectively modulate the catalytic sites, chemisorption energy of O₂ molecules, and local electronic structure of carbon materials, leading to enhanced ORR activity.^[24–28,57,58] As shown in Figure S4 (Supporting Information), the ORR activity of the as-obtained CGHNs is very poor. Thermal reduction with H₂ can improve the ORR performance due to the increased electronic conductivity. Doping with N or P could further effectively promote the electrocatalytic activity of the nanospheres. But they still need to be improved to become comparable with Pt/C and meet the requirement for practical applications. Recent studies show that multiple-element doping is better than single-element doping for improving the electrochemical activities.^[59–63] Note that N and P dual-doped carbon materials have been proved to exhibit superior ORR performance recently.^[64–68] As obtained nanospheres were then doped with N and P to explore their ORR activity. They were first

subjected to thermal treatment under NH₃ to make N-doped CGHNs. P element was then introduced into the above materials by reannealing with triphenylphosphine under Ar atmosphere to achieve N,P-CGHNs. Elemental analysis indicated that the carbon, nitrogen, phosphorus, and oxygen contents in N,P-CGHNs prepared from 1:1 mass ratio of CNT/graphene are 92.69, 3.26, 0.05, and 3.9 wt%, respectively. Electrochemical measurements (Figure S4, Supporting Information) confirmed that N,P-doped samples exhibited much higher catalytic activity toward ORR compared to those only doped with either N or P. The possible reason is that additional doping a small amount of P element which is a good electron donor into N-doped carbon can enhance the charge delocalization and asymmetric spin density of carbon atoms and can also increase active sites for ORR.^[34,66] Therefore, N-doping and P-doping could synergistically enhance the electrocatalytic activity for ORR. No obvious structural changes can be observed from SEM images after sequential thermal treatment as shown in Figure S5 (Supporting Information). According to powder X-ray diffraction patterns (Figure S6, Supporting Information), the peak at $2\theta = 26^\circ$ corresponding to crystalline carbon structures remained unchanged after doping. Such hybrid nanospheres are very robust and highly stable due to strong π - π interaction between

CNTs and graphene. They still maintained integral structures even after 30 min sonication in water using a 150 W ultrasonicator (Figure S7, Supporting Information). This unique feature renders N,P-CGHNs to show excellent stability when used as electrocatalysts for ORR in aqueous electrolytes.

Raman characterization showed that N,P-CGHNs exhibited much higher I_D/I_G ratios compared to pristine mixtures of oxidized CNTs and GOs and CGHNs, indicating more defects and edge sites were created after doping (Figure S8, Supporting Information). XPS measurements were conducted to investigate the surface chemical composition of N,P-CGHNs prepared from different mass ratios of CNT/graphene. From Table S2 (Supporting Information), we can see that as-prepared N,P-CGHNs contained different amounts of C, N, P, and O, indicating both N and P atoms were doped into the carbon skeleton. The presence of oxygen could be ascribed to the remaining oxygen-containing functional groups and physicochemically adsorbed small molecules (e.g., H_2O , CO_2 , and O_2) on nanospheres.^[13,15,65] High resolution XPS spectra can provide more information about the bonding configuration of the dopants. Therefore, the N 1s and P 2p spectra were further deconvoluted to reveal the bonding information of N and P elements. For example, various nitrogen bonding states such as pyridinic N (398.3 eV) (46.5%), amine N (399.4 eV) (10.7%), pyrrolic N (400.1 eV) (17.8%), and graphitic N (401.4 eV) (25%) can be distinguished from the high resolution N 1s spectrum in N,P-CGHNs prepared from 1:1 mass ratio of CNT/graphene (Figure S9c, Supporting Information). Both pyridinic and graphitic N were generally considered as efficient active sites for oxygen reduction.^[15,19] The high content of pyridinic (46.5%) and graphitic N (25%) thus should be beneficial for enhancing ORR activity. Elemental mapping revealed that the incorporated nitrogen and phosphorus atoms were homogeneously distributed in the entire nanospheres (Figure S10, Supporting Information). The P 2p spectrum (Figure S9d, Supporting Information) was deconvoluted into two peaks located at 133 eV and 134 eV, which can be ascribed to P—C and P—O bonding, respectively.^[34,64–66] N,P dual-doped carbon could further lower the charge-transfer resistance compared to those only doped with N or P as revealed by electrochemical impedance spectroscopy (EIS) measurements, which is desired for improving ORR activity (Figure S11, Supporting Information).

N,P-CGHNs prepared from different mass ratios of CNT/graphene were initially screened by rotating disk electrode (RDE) measurements in 0.1 M KOH and 0.1 M $HClO_4$ to compare their ORR performance. The highest ORR activity was observed for N,P-CGHNs with 1:1 mass ratio of CNT/graphene in terms of the onset potential (E_{onset}), half-wave potential ($E_{1/2}$), and diffusion-limiting current (Figure S12, Supporting Information). This could be due to the highest specific surface area (Figure S13, Supporting Information), lowest charge-transfer resistance (Figure S14, Supporting Information), and optimal heteroatom doping (Table S2, Supporting Information) formed at this mass ratio. Therefore, in the following section, we mainly discuss the ORR performance of N,P-CGHNs prepared from 1:1 mass ratio of CNT/graphene unless otherwise specified.

To examine the electrocatalytic activity of N,P-CGHNs in alkaline media, cyclic voltammetry (CV) measurements were carried out in O_2 - and Ar-saturated 0.1 M KOH. A commercial

Pt/C catalyst (20 wt%, Johnson Matthey) was used for comparison. As shown in Figure S15 (Supporting Information), the CV curves exhibit a pronounced peak in O_2 -saturated electrolyte whereas only featureless double-layer charging current can be observed in Ar-saturated electrolyte, implying that these catalysts possess ORR activity. The peak potential at 0.820 V versus reversible hydrogen electrode (RHE) afforded by N,P-CGHNs is comparable to that of Pt/C (0.824 V). The linear-sweep voltammetric (LSV) curves in Figure 3a confirm that N,P-CGHNs exhibit prominent electrocatalytic performance with an E_{onset} of 0.94 V vs RHE and an $E_{1/2}$ of 0.82 V vs RHE. These values are higher than those of Pt/C tested under the same conditions ($E_{onset} = 0.93$ V and $E_{1/2} = 0.81$ V), and outperform most previously reported metal-free ORR catalysts (Table S3, Supporting Information). The electron transfer number (n) per oxygen molecule for ORR can be calculated from the LSV curves according to the Koutechy–Levich (K–L) equation (Figure 3b). And the value of n is determined to be 4, suggesting a four-electron pathway for ORR.

To further evaluate the ORR performance of the N,P-CGHNs catalyst, we conducted rotating ring-disk electrode (RRDE) measurements. As shown in Figure 3c, the E_{onset} and $E_{1/2}$ of N,P-CGHNs are superior to those of Pt/C. The diffusion-limiting current also suggests a better performance of N,P-CGHNs (e.g., 5.90 mA cm^{-2} at 0.2 V vs RHE) than that of Pt/C (5.28 mA cm^{-2}). The average electron transfer number calculated from the RRDE measurements at all potentials is 3.95, which is close to the value calculated from Pt/C (3.94), further confirming the desired four-electron oxygen reduction process. RRDE results indicate that the H_2O_2 yield measured with the N,P-CGHNs remained below 6% at all potentials and dropped to 0.6% at 0.8 V vs RHE, indicating N,P-CGHNs have extremely high ORR catalytic efficiency. N,P-CGHNs also show high stability for ORR, as confirmed by the absence of an ORR polarization curve shift after 5000 cycles (Figure 3e), while there is a 40 mV loss of $E_{1/2}$ for the Pt/C catalyst under the same conditions (Figure S16, Supporting Information). In addition, the tolerance of the N,P-CGHNs and Pt/C catalysts toward MeOH was determined by adding 1.0 M MeOH into 0.1 M KOH electrolyte. CV curves (Figure S17a, Supporting Information) for N,P-CGHNs show no obvious change with the addition of MeOH. By contrast, typical methanol oxidation behavior can be observed on Pt/C catalyst in the presence of MeOH in 0.1 M KOH (Figure S17b, Supporting Information). The LSV curves (Figure 3f) for N,P-CGHNs show negligible variation with the addition of 1 M MeOH, but a negative shift of 70 mV in $E_{1/2}$ for the Pt/C catalyst can be observed (Figure S18, Supporting Information). These results suggest that N,P-CGHNs have much better selectivity and stability than the commercial Pt/C catalyst.

Up to now, very few reports on metal-free electrocatalysts have shown high ORR performance in both alkaline and acidic media.^[29,30,40,45,64] Interestingly, our N,P-CGHNs are also active and durable for ORR in acidic electrolyte. The CV curves indicate a significant reduction process occurred for N,P-CGHNs, with a pronounced cathodic ORR peak at 0.63 V vs RHE in O_2 -saturated 0.1 M $HClO_4$ (Figure S19, Supporting Information). As shown in Figure 4a, in 0.1 M $HClO_4$ solution, the ORR polarization curve of N,P-CGHNs exhibits a high E_{onset} (≈ 0.90 V) which is close to that of the Pt/C catalyst (0.96 V)

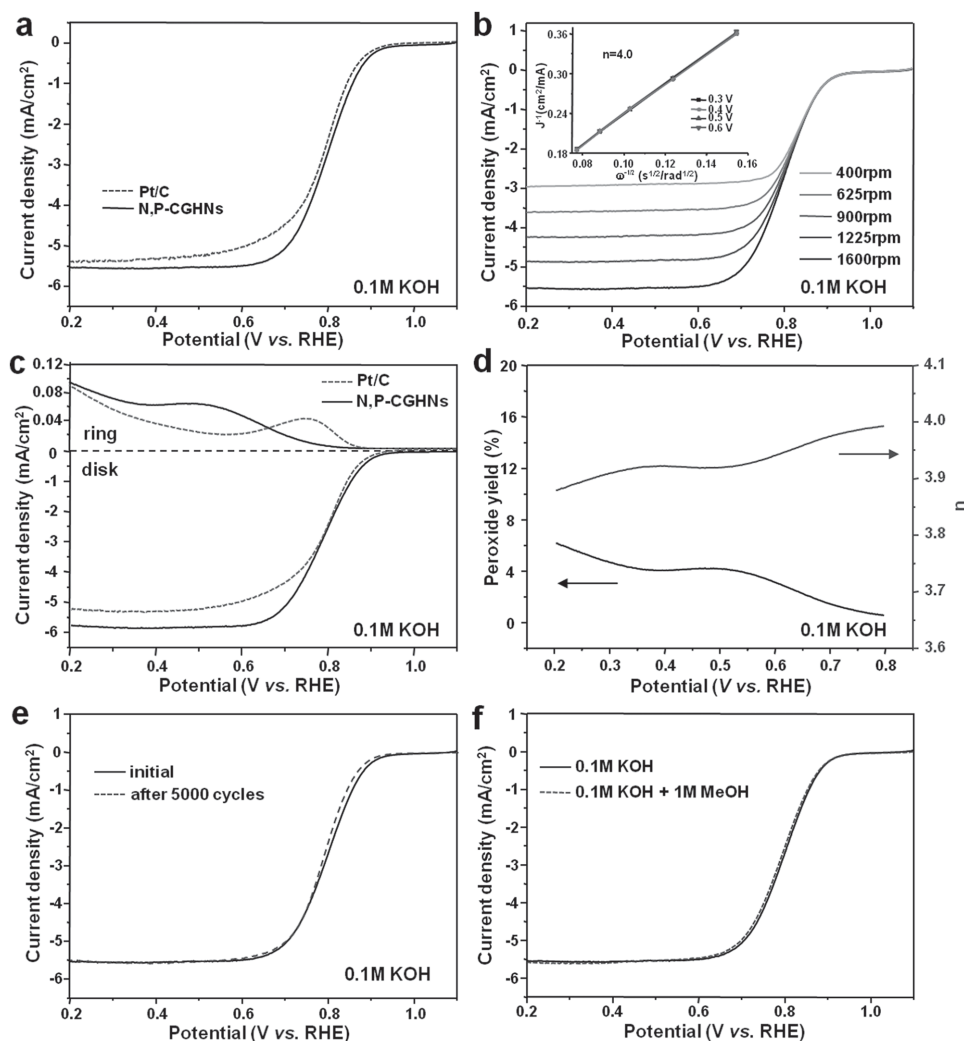


Figure 3. a) LSV curves of N,P-CGHNs and Pt/C in O₂-saturated 0.1 M KOH. b) LSV curves of N,P-CGHNs in O₂-saturated 0.1 M KOH at various rotation speeds. c) RRDE voltammograms and (d) peroxide yield with regard to the total oxygen reduction products and the calculated electron transfer number of N,P-CGHNs and Pt/C in O₂-saturated 0.1 M KOH. e) Durability test of the N,P-CGHNs catalyst for 5000 cycles in O₂-saturated 0.1 M KOH. f) LSV curves of N,P-CGHNs in O₂-saturated 0.1 M KOH with and without 1 M MeOH. Electrode rotation speed: 1600 rpm; scan rate: 10 mV s⁻¹.

and the difference in $E_{1/2}$ is only 70 mV. Compared to other metal-free and nonprecious metal-based ORR catalysts reported in the literature, our catalyst exhibits one of the highest electrocatalytic ORR activities (Table S4, Supporting Information). The electron transfer number of N,P-CGHNs derived from K-L plots (Figure 4b) is 3.9, indicating a four-electron pathway dominated the ORR process. RRDE polarization curves (Figure 4c) also reveal comparable E_{onset} for N,P-CGHNs and Pt/C catalyst. The H₂O₂ yield on the N,P-CGHNs in acidic solution is below 10% over the measured potential range (Figure 4d). The average electron transfer number calculated from the RRDE measurements at all potentials is 3.9, which is close to the value calculated from Pt/C (3.95). The polarization curve recorded after 5000 cycles shows a negative shift of $E_{1/2}$ of 20 mV for N,P-CGHNs catalyst (Figure 4e), while there is a 140 mV loss of $E_{1/2}$ for the Pt/C catalyst under the same conditions (Figure S20, Supporting Information), indicating the durability of N,P-CGHNs catalyst is superior to that of Pt/C. In fact, our N,P-CGHNs

catalyst can outperform the commercial Pt/C catalyst after 5000 cycles, as determined from LSV curves (Figure S21, Supporting Information). N,P-CGHNs were also tested for the possible crossover effect caused by MeOH. Obviously, the peak current for N,P-CGHNs remains unchanged in the presence of MeOH (Figure S22a, Supporting Information), whereas Pt/C shows a significant MeOH oxidation current (Figure S22b, Supporting Information), implying that our metal-free N,P-CGHNs catalyst shows high selectivity for ORR with strong tolerance to crossover effect in acidic solution.

Previously, CNT/graphene complexes synthesized from oxidation of few-walled carbon nanotubes showed that high ORR activity actually originated from iron-containing active sites formed during synthesis.^[46] Purified carbon nanotube-graphene complexes exhibited significantly lower ORR activity. We then investigated whether the trace amount of iron species (≈ 0.09 wt%, as determined from inductively coupled plasma mass spectrometry (ICP-MS)) in our N,P-CGHNs could be the

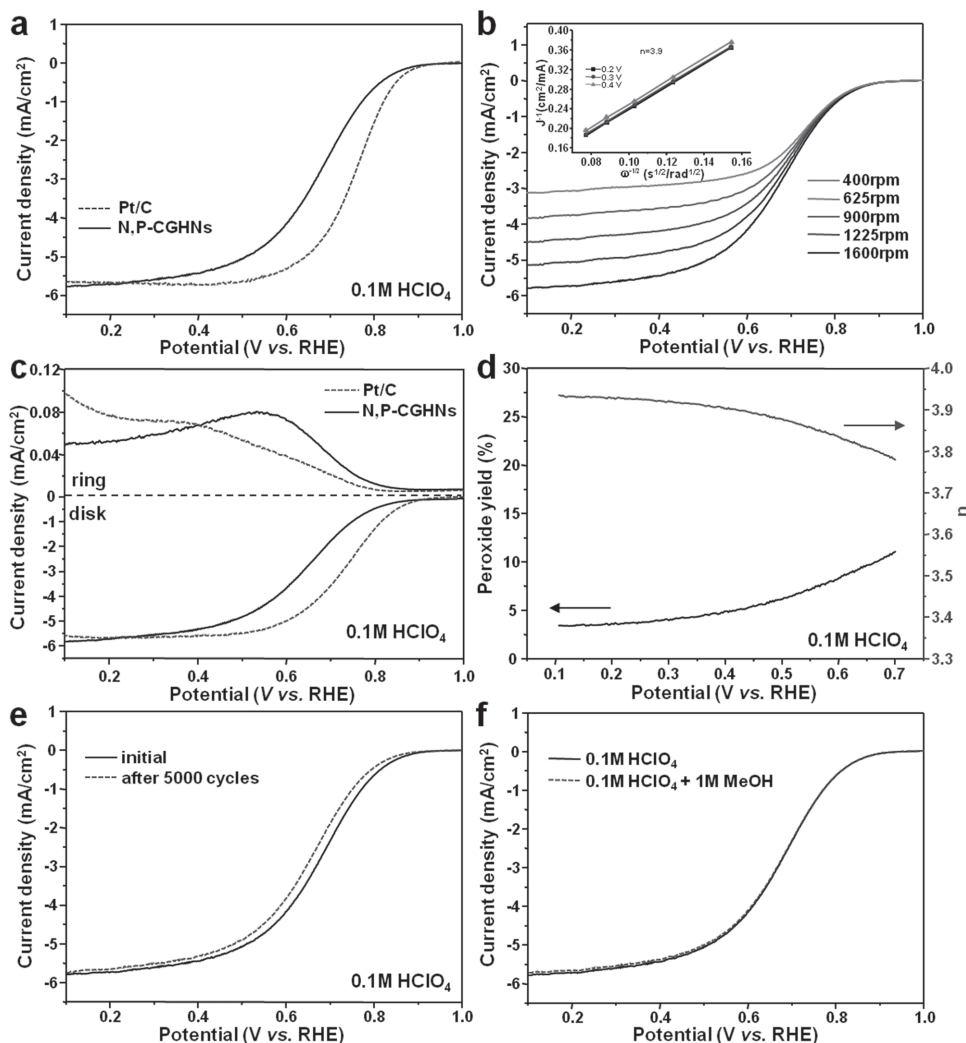


Figure 4. a) LSV curves of N,P-CGHNs and Pt/C in O_2 -saturated 0.1 M $HClO_4$. b) LSV curves of N,P-CGHNs in O_2 -saturated 0.1 M $HClO_4$ at various rotation speeds. c) RRDE voltammograms and (d) peroxide yield with regard to the total oxygen reduction products and the calculated electron transfer number of N,P-CGHNs and Pt/C in O_2 -saturated 0.1 M $HClO_4$. e) Durability test of the N,P-CGHNs catalyst for 5000 cycles in O_2 -saturated 0.1 M $HClO_4$. f) LSV curves of N,P-CGHNs in O_2 -saturated 0.1 M $HClO_4$ with and without 1 M MeOH. Electrode rotation speed: 1600 rpm; scan rate: 10 mV s^{-1} .

cause for the exceptional ORR performance. Thiocyanate ions (SCN^-) are known to coordinate with iron species to form stable complexes and hence poison the iron-containing catalytic sites in acidic conditions. If iron species are the actual sites for ORR, the activity will be suppressed upon adding SCN^- ions.^[69] As shown in Figure S23 (Supporting Information), SCN^- ions in 0.1 M $HClO_4$ solution have negligible influence on the ORR performance for our N,P-CGHNs catalyst. This study strongly suggests that trace iron residues do not contribute to the ORR activity.^[70]

To further demonstrate the advantages of using these unique N,P-CGHNs produced via aerosol-assisted assembling approach in ORR, the electrocatalytic performance of N,P-doped CNT/graphene hybrid materials prepared using other common methods such as hydrothermal process^[42] and sol-cryo method^[49] is examined under the same conditions. As shown in Figure S24 (Supporting Information), the ORR polarization curves of N,P-CGHNs exhibit much higher E_{onset} and $E_{1/2}$ compared to the N,P-doped CNT/graphene hybrid materials prepared using

other methods. EIS measurements (Figure S25, Supporting Information) reveal that the N,P-CGHNs exhibit much smaller charge transfer resistance compared to the N,P-doped CNT/graphene hybrid materials prepared using hydrothermal process or “sol-cryo” method. Therefore, our study clearly indicates that N,P-CGHNs assembled using the aerosol method are very efficient in shuttling electrons from electrode to solution, and the electrocatalytic activity for ORR is superior to those CNT/graphene hybrid materials synthesized using other methods.

Finally, we constructed a Zn-air battery to evaluate the potential of our catalyst for real energy conversion devices. Commercial Pt/C catalysts were also tested under the same conditions for comparison. Open-circuit voltages of 1.50 and 1.49 V were measured for N,P-CGHNs and Pt/C, respectively (Figure S26, Supporting Information), suggesting that N,P-CGHNs performed as a very good electrocatalyst for ORR under practical conditions. Galvanostatic discharge tests at 5 and 25 mA cm^{-2} showed that the performance of

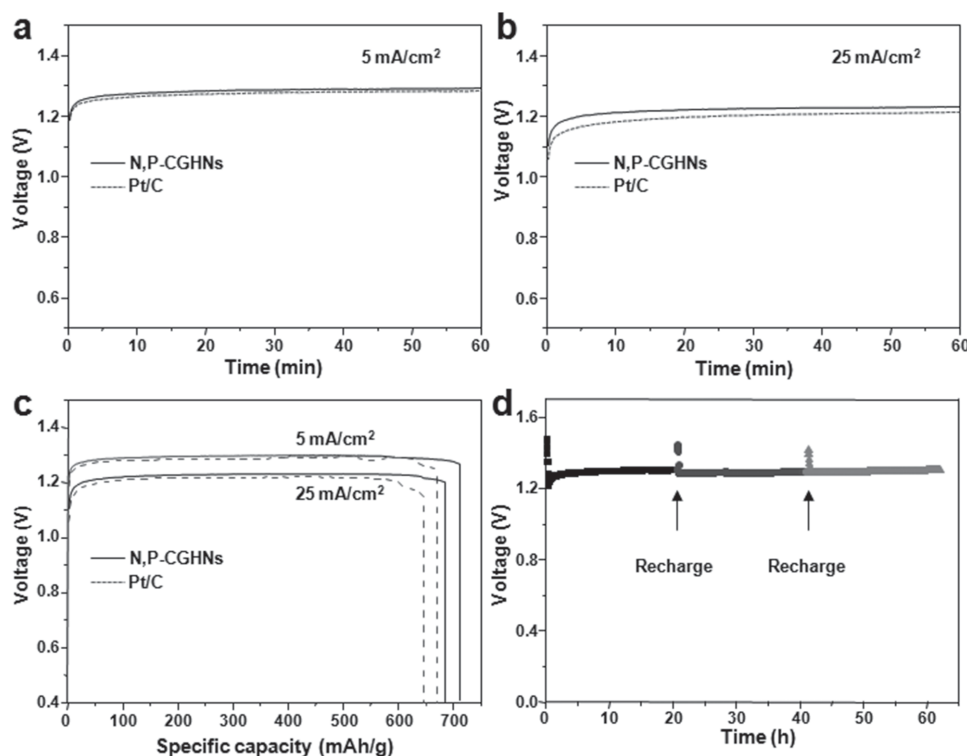


Figure 5. a,b) Galvanostatic discharge curves of Zn–air batteries with N,P-CGHNs and Pt/C as cathode catalysts at two different current densities: (a) 5 mA cm^{-2} and (b) 25 mA cm^{-2} . c) Long-term galvanostatic discharge curves of Zn–air batteries with N,P-CGHNs and Pt/C as cathode catalysts until complete consumption of the Zn anode. The specific capacity was normalized to the mass of consumed Zn. d) Long-time durability of the Zn–air battery using N,P-CGHNs catalyst at a current density of 2 mA cm^{-2} . The battery can be recharged by replenishing the Zn anode and the electrolyte. The recharging process is indicated by an arrow.

N,P-CGHNs-based Zn–air battery was superior to that of Pt/C-based Zn–air battery (Figure 5a,b). The specific capacity of N,P-CGHNs-based battery normalized to the mass of consumed Zn was 712 mAh g^{-1} at the discharge density of 5 mA cm^{-2} (corresponding to an energy density of $\approx 872 \text{ Wh kg}^{-1}$) (Figure 5c). When the current density was increased to 25 mA cm^{-2} , the specific capacity of the battery was 684 mAh g^{-1} (corresponding to an energy density of $\approx 781 \text{ Wh kg}^{-1}$). These values are higher than those of Zn–air batteries using Pt/C catalyst (833 Wh kg^{-1} at 5 mA cm^{-2} , 744 Wh kg^{-1} at 25 mA cm^{-2}), an indication of excellent catalytic performance of N,P-CGHNs loaded on the air electrode. After complete discharging, the battery can be recovered by refueling the Zn anode and electrolyte periodically without visible voltage loss (Figure 5d), highlighting again the excellent stability of the N,P-CGHNs catalyst.

In conclusion, we have demonstrated a facile route to assemble CNTs and graphene into robust hybrid nanospheres as a new class of metal-free electrocatalyst for ORR. Integration of CNTs and graphene into the hybrid nanospheres can synergistically enhance the electronic conductivity and increase the specific surface area. After doping with nitrogen and phosphorus, such prepared hybrid nanospheres are found to exhibit higher ORR activity, better stability, and better methanol tolerance for ORR than the commercial Pt/C catalyst in alkaline solution. In addition, our new hybrid catalyst also shows a comparable ORR onset potential and much better stability than the commercial Pt/C catalyst in acidic solution. When used as an

ORR catalyst in the air electrode for Zn–air battery, our metal-free catalyst can outperform the state-of-the-art Pt/C catalyst. Our study provides a new synthetic method and design strategy for preparing novel metal-free ORR electrocatalysts from CNTs and graphene for electrochemical energy conversion devices.

Supporting Information

Supporting Information is available from the Wiley Online Library or from the author.

Acknowledgements

J.Y. and H.S. contributed equally to this work. This work was supported by the National Key Basic Research Program of China (Grant No. 2015CB351903), the National Natural Science Foundation of China (Grant Nos. 51402282, 21474095, 11272303, 51533008, and 21325417), and the Fundamental Research Funds for the Central Universities.

Received: November 25, 2015

Revised: February 18, 2016

Published online: April 8, 2016

- [1] M. K. Debe, *Nature* **2012**, *486*, 43.
- [2] I. Katsounaros, S. Cherevko, A. R. Zeradjanin, K. J. J. Mayrhofer, *Angew. Chem. Int. Ed.* **2014**, *53*, 102.

- [3] X. Ge, A. Sumboja, D. Wu, T. An, B. Li, F. W. T. Goh, T. S. A. Hor, Y. Zong, Z. Liu, *ACS Catal.* **2015**, *5*, 4643.
- [4] H. A. Gasteiger, S. S. Kocha, B. Sompalli, F. T. Wagner, *Appl. Catal. B.* **2005**, *56*, 9.
- [5] J. Wu, H. Yang, *Acc. Chem. Res.* **2013**, *46*, 1848.
- [6] J. Greeley, I. E. L. Stephens, A. S. Bondarenko, T. P. Johansson, H. A. Hansen, T. F. Jaramillo, J. Rossmeisl, I. Chorkendorff, J. K. Nørskov, *Nat. Chem.* **2009**, *1*, 552.
- [7] Y. Nie, L. Li, Z. Wei, *Chem. Soc. Rev.* **2015**, *44*, 2168.
- [8] Y. Bing, H. Liu, L. Zhang, D. Ghosha, J. Zhang, *Chem. Soc. Rev.* **2010**, *39*, 2184.
- [9] J. C. Meier, I. Katsounaros, C. Galeano, H. J. Bongard, A. A. Topalov, A. Kostka, A. Karschin, F. Schüth, K. J. J. Mayrhofer, *Energy Environ. Sci.* **2012**, *5*, 9319.
- [10] X. Yu, S. Ye, *J. Power Sources* **2007**, *172*, 133.
- [11] R. Borup, J. Meyers, B. Pivovar, Y. S. Kim, R. Mukundan, N. Garland, D. Myers, M. Wilson, F. Garzon, D. Wood, P. Zelenay, K. More, K. Stroh, T. Zawodzinski, J. Boncella, J. E. McGrath, M. Inaba, K. Miyatake, M. Hori, K. Ota, Z. Ogumi, S. Miyata, A. Nishikata, Z. Siroma, Y. Uchimoto, K. Yasuda, K. Kimijima, N. Iwashita, *Chem. Rev.* **2007**, *107*, 3904.
- [12] J. Masa, W. Xia, M. Muhler, W. Schuhmann, *Angew. Chem. Int. Ed.* **2015**, *54*, 10102.
- [13] Z. Xiang, D. Cao, L. Huang, J. Shui, M. Wang, L. Dai, *Adv. Mater.* **2014**, *26*, 3315.
- [14] D. Zhao, J. L. Shui, L. R. Grabstanowicz, C. Chen, S. M. Commet, T. Xu, J. Lu, D. J. Liu, *Adv. Mater.* **2014**, *26*, 1093.
- [15] Z. S. Wu, L. Chen, J. Liu, K. Parvez, H. Liang, J. Shu, H. Sachdev, R. Graf, X. Feng, K. Mullen, *Adv. Mater.* **2014**, *26*, 1450.
- [16] Z. Chen, D. Higgins, A. Yu, L. Zhang, J. Zhang, *Energy Environ. Sci.* **2011**, *4*, 3167.
- [17] M. Lefevre, E. Proietti, F. Jaouen, J. P. Dodelet, *Science* **2009**, *324*, 71.
- [18] G. Wu, K. L. More, C. M. Johnston, P. Zelenay, *Science* **2011**, *332*, 443.
- [19] L. Lin, Q. Zhu, A. W. Xu, *J. Am. Chem. Soc.* **2014**, *136*, 11027.
- [20] H. Fei, R. Ye, G. Ye, Y. Gong, Z. Peng, X. Fan, E. L. G. Samuel, P. M. Ajayan, J. M. Tour, *ACS Nano* **2014**, *8*, 10837.
- [21] W. Niu, L. Li, X. Liu, N. Wang, J. Liu, W. Zhou, Z. Tang, S. Chen, *J. Am. Chem. Soc.* **2014**, *137*, 5555.
- [22] Q. Lin, X. Bu, A. Kong, C. Mao, F. Bu, P. Feng, *Adv. Mater.* **2015**, *27*, 3431.
- [23] M. Xiao, J. Zhu, L. Feng, C. Liu, W. Xing, *Adv. Mater.* **2015**, *27*, 2521.
- [24] L. Dai, Y. Xue, L. Qu, H. J. Choi, J. B. Baek, *Chem. Rev.* **2015**, *115*, 4823.
- [25] D.-W. Wang, D. Su, *Energy Environ. Sci.* **2014**, *7*, 576.
- [26] Z. Zhao, M. Li, L. Zhang, L. Dai, Z. Xia, *Adv. Mater.* **2015**, *27*, 6834.
- [27] J. Duan, S. Chen, M. Jaroniec, S. Z. Qiao, *ACS Catal.* **2015**, *5*, 5207.
- [28] H. Shi, Y. Shen, F. He, Y. Li, A. Liu, S. Liu, Y. Zhang, *J. Mater. Chem. A.* **2014**, *2*, 15704.
- [29] H. Liang, X. Zhuang, S. Brüller, X. Feng, K. Müllen, *Nat. Commun.* **2014**, *5*, 4973.
- [30] W. Wei, H. Liang, K. Parvez, X. Zhuang, X. Feng, K. Mullen, *Angew. Chem. Int. Ed.* **2014**, *53*, 1570.
- [31] W. Ding, Z. Wei, S. Chen, X. Qi, T. Yang, J. Hu, D. Wang, L. J. Wan, S. F. Alvi, L. Li, *Angew. Chem. Int. Ed.* **2013**, *52*, 11755.
- [32] L. Hao, S. Zhang, R. Liu, J. Ning, G. Zhang, L. Zhi, *Adv. Mater.* **2015**, *27*, 3190.
- [33] S. Chen, J. Bi, Y. Zhao, L. Yang, C. Zhang, Y. Ma, Q. Wu, X. Wang, Z. Hu, *Adv. Mater.* **2012**, *24*, 5593.
- [34] D. S. Yang, D. Bhattacharjya, S. Inamdar, J. Park, J. S. Yu, *J. Am. Chem. Soc.* **2012**, *134*, 16127.
- [35] R. Silva, D. Voiry, M. Chhowalla, T. Asefa, *J. Am. Chem. Soc.* **2013**, *135*, 7823.
- [36] I. Y. Jeon, H. J. Choi, S. M. Jung, J. M. Seo, M. J. Kim, L. Dai, J. B. Baek, *J. Am. Chem. Soc.* **2013**, *135*, 1386.
- [37] Q. Shi, F. Peng, S. Liao, H. Wang, H. Yu, Z. Liu, B. Zhang, D. Su, *J. Mater. Chem. A* **2013**, *1*, 14853.
- [38] H. Zhong, J. Wang, Y. Zhang, W. Xu, W. Xing, D. Xu, Y. Zhang, X. Zhang, *Angew. Chem. Int. Ed.* **2014**, *53*, 14235.
- [39] Y. Li, Y. Zhao, H. Cheng, Y. Hu, G. Shi, L. Dai, L. Qu, *J. Am. Chem. Soc.* **2012**, *134*, 15.
- [40] K. Ai, Y. Liu, C. Ruan, L. Lu, G. Lu, *Adv. Mater.* **2013**, *25*, 998.
- [41] N. Alexeyeva, E. Shulga, V. Kisand, I. Kink, K. Tammeveski, *J. Electroanal. Chem.* **2010**, *648*, 169.
- [42] P. Chen, T. Y. Xiao, Y. H. Qian, S. S. Li, S. H. Yu, *Adv. Mater.* **2013**, *25*, 3192.
- [43] N. Jung, S. Kwon, D. Lee, D.-M. Yoon, Y. M. Park, A. Benayad, J.-Y. Choi, J. S. Park, *Adv. Mater.* **2013**, *25*, 6854.
- [44] G. L. Tian, M. Q. Zhao, D. Yu, X. Y. Kong, J. Q. Huang, Q. Zhang, F. Wei, *Small* **2014**, *10*, 2251.
- [45] J. Shui, M. Wang, F. Du, L. Dai, *Sci. Adv.* **2015**, *1*, e1400129.
- [46] Y. Li, W. Zhou, H. Wang, L. Xie, Y. Liang, F. Wei, J. C. Idrobo, S. J. Pennycook, H. Dai, *Nat. Nanotechnol.* **2012**, *7*, 394.
- [47] S. Ratsio, I. Kruusenberg, M. Vikkisk, U. Joost, E. Shulga, I. Kink, T. Kallio, K. Tammeveski, *Carbon* **2014**, *73*, 361.
- [48] B. C. H. Steele, A. Heinzl, *Nature* **2001**, *414*, 345.
- [49] H. Sun, Z. Xu, C. Gao, *Adv. Mater.* **2013**, *25*, 2554.
- [50] J. H. Bang, K. S. Suslick, *Adv. Mater.* **2010**, *22*, 1039.
- [51] J. Luo, H. D. Jang, T. Sun, L. Xiao, Z. He, A. P. Katsoulidis, M. G. Kanatzidis, J. M. Gibson, J. Huang, *ACS Nano* **2011**, *5*, 8943.
- [52] X. Ma, M. R. Zachariah, C. Zangmeister, *Nano Lett.* **2012**, *12*, 486.
- [53] J. J. Shao, W. Lv, Q. H. Yang, *Adv. Mater.* **2014**, *26*, 5586.
- [54] Y. Chen, F. Guo, A. Jachak, S.-P. Kim, D. Datta, J. Liu, I. Kulaots, C. Vaslet, H. D. Jang, J. Huang, A. Kane, V. B. Shenoy, R. H. Hurt, *Nano Lett.* **2012**, *12*, 1996.
- [55] S. Mao, Z. Wen, H. Kim, G. Lu, P. Hurley, J. Chen, *ACS Nano* **2012**, *6*, 7505.
- [56] Y. Chen, F. Guo, Y. Qiu, H. Hu, I. Kulaots, R. H. Hurt, *ACS Nano* **2013**, *7*, 3744.
- [57] Y. Jiao, Y. Zheng, M. Jaroniec, S. Z. Qiao, *J. Am. Chem. Soc.* **2014**, *136*, 4394.
- [58] J. Y. Cheon, J. H. Kim, J. H. Kim, K. C. Goddeti, J. Y. Park, S. H. Joo, *J. Am. Chem. Soc.* **2014**, *136*, 8875.
- [59] Y. Zheng, Y. Jiao, L. Ge, M. Jaroniec, S. Z. Qiao, *Angew. Chem. Int. Ed.* **2013**, *52*, 3110.
- [60] S. Chen, J. Duan, M. Jaroniec, S. Z. Qiao, *Adv. Mater.* **2014**, *26*, 2925.
- [61] W. Ai, Z. Luo, J. Jiang, J. Zhu, Z. Du, Z. Fan, L. Xie, H. Zhang, W. Huang, T. Yu, *Adv. Mater.* **2014**, *26*, 6186.
- [62] C. H. Choi, M. W. Chung, H. C. Kwon, S. H. Park, S. I. Woo, *J. Mater. Chem. A.* **2013**, *1*, 3694.
- [63] Y. Meng, D. Voiry, A. Goswami, X. Zou, X. Huang, M. Chhowalla, Z. Liu, T. Asefa, *J. Am. Chem. Soc.* **2014**, *136*, 13554.
- [64] J. Zhang, Z. Zhao, Z. Xia, L. Dai, *Nat. Nanotechnol.* **2015**, *10*, 444.
- [65] W. Zhang, Z. Y. Wu, H. L. Jiang, S. H. Yu, *J. Am. Chem. Soc.* **2014**, *136*, 14385.
- [66] R. Li, Z. Wei, X. Gou, *ACS Catal.* **2015**, *5*, 4133.
- [67] X. Gong, S. Liu, C. Ouyang, P. Strasser, R. Yang, *ACS Catal.* **2015**, *5*, 920.
- [68] H. Jiang, Y. Zhu, Q. Feng, Y. Su, X. Yang, C. Li, *Chem. Eur. J.* **2014**, *20*, 3106.
- [69] Q. Wang, Z.-Y. Zhou, Y.-J. Lai, Y. You, J.-G. Liu, X.-L. Wu, E. Terefe, C. Chen, L. Song, M. Rauf, N. Tian, S.-G. Sun, *J. Am. Chem. Soc.* **2014**, *136*, 10882.
- [70] K. Waki, R. A. Wong, H. S. Oktaviano, T. Fujio, T. Nagai, K. Kimoto, K. Yamada, *Energy Environ. Sci.* **2014**, *7*, 1950.